Two-Stage Stochastic Optimization Meets Two-Scale Simulation

Sergio Conti, Benedict Geihe, Martin Rumpf, and Rüdiger Schultz

Abstract Risk averse stochastic optimization is investigated in the context of elastic shape optimization, allowing for microstructures in the admissible shapes. In particular, a two-stage model for shape optimization under stochastic loading with risk averse cost functionals is combined with a two-scale approach for the simulation of microstructured materials. The microstructure is composed of an elastic material with geometrically simple perforations located on a regular periodic lattice. Different types of microscopic geometries are investigated and compared to each other. In addition they are compared to optimal nested laminates, known to realize the optimal lower bound of compliance cost functionals. We combine this two-scale approach to elastic shapes with a two-stage stochastic programming approach to risk averse shape optimization, dealing with risk neutral and risk averse cost functionals in the presence of stochastic loadings.

Keywords Two-stage stochastic programming • Risk averse optimization • Two-scale elastic shape optimization • Microstructure optimization • Finite element method • Boundary element method

Mathematics Subject Classification (2010). 90C15, 74B05, 74P05, 74Q05, 74S05, 74S15, 49M29.

S. Conti
Institut für Angewandte Mathematik, Universität Bonn, Endenicher Allee 60, 53115 Bonn, Germany
e-mail: sergio.conti@uni-bonn.de

B. Geihe (✉) • M. Rumpf
Institut für Numerische Simulation, Universität Bonn, Endenicher Allee 60, 53115 Bonn, Germany
e-mail: benedict.geihe@ins.uni-bonn.de; martin.rumpf@ins.uni-bonn.de

R. Schultz
Fakultät für Mathematik, Universität Duisburg-Essen, Thea-Leymann-Str. 9, D-45117 Essen, Germany
e-mail: ruediger.schultz@uni-due.de

G. Leugering et al. (eds.), *Trends in PDE Constrained Optimization*, International Series of Numerical Mathematics 165, DOI 10.1007/978-3-319-05083-6_13

1 Introduction

In nature, when biological material has to resist strong mechanical loading, fine scale structures frequently characterize the material. Prominent examples are the microstructure of wood [5] or the substantia spongiosa of bones [35]. The pattern formed by these elastic structures is not uniform but varies spatially. This spatial variation seems to be adapted to the local load configuration, which supports the hypothesis of nature optimizing mechanical structures in the ontogenesis [45]. Thus, a natural question arises, what are "optimal" microstructures, which are observable in nature or can be used in the design of mechanical devices. When optimizing material structures one has to take into account that load configurations in nature and in engineering are usually not deterministic but stochastic.

This paper addresses the optimization of microstructures in elastic materials under stochastic loading. It is well known that microstructures form when minimizing compliance or tracking type cost functionals, unless a penalty on the area of material interfaces is taken into account. The optimal microstructures are well-understood and can be represented by nested laminates [1]. The laminate construction is an analytically elegant tool but can hardly be reproduced in mechanical devices, nor is it observed in optimization problems posed in nature. Thus, the question arises how close one can get to the optimal design with constructible microstructures. To this end, different types of parametrized microstructures will be investigated and compared.

2 Related Work

Shape optimization under deterministic loading has extensively been investigated in the literature. For an overview we refer to the textbooks [1, 13]. Most approaches deal with a macroscopic shape description under the assumption of sufficient shape regularity, which is usually guaranteed by an additional regularizing cost functional such as the shape perimeter. If only scale invariant cost functionals are taken into account, then in general an optimal shape will not exist. Indeed, minimizing sequences of shapes will be characterized by very fine microstructures. The theory of homogenization allows to describe the set of possible microstructures and the associated set of attainable effective material properties [20, 21, 23, 36]. The heterogeneous multi-scale method (HMM) [49, 50] depicts a very general paradigm for efficient numerical treatment of multi-scale problems using independent macroscopic and microscopic models. Homogenization theory was extended from multiphase, uniformly coercive materials to perforated structures and porous materials, see for example [24] and references therein. In [34] a two-scale adaptive finite element scheme has been proposed for elliptic problems on perforated domains.

Optimal microstructures in elasticity have first been derived by Hashin in 1962 [31] in the concentric sphere construction for hydrostatic loads. The construction was later generalized for anisotropic strains using confocal ellipsoids in [29]. The investigation of nested laminate structures dates back to the 1980s [40, 46] and was later used in a practical numerical scheme for topology optimization in [2]. In all these cases proofs of optimality rely on the Hashin-Shtrikman bounds on the attainable sets of effective elastic properties [32]. Related to the homogenization approach is the so called free material optimization method where the optimization is directly carried out on the coefficients of the elasticity tensor, as for example in [33].

Alternatively, the cost functional can be reduced by a proper design of fine scale perforations drilled into a homogeneous material. The layout of elastic structures based on this approach has been investigated already in the early 1990s [14]. The shape optimization via such mechanically feasible, periodic perforation patterns on the microscale has also been studied in [9]. Closely related to our approach is the approach by Barbarosie and Toader. In [10, 11] they optimized the geometry of fine scale perforations. The numerical method is based on a boundary tracking approach of a triangulated domain with additional remeshing steps to ensure mesh quality. In [12] this approach is extended to a two-scale setting combining a finite element scheme on the macroscale with the above treatment of locally periodic perforations on the microscale.

Shape optimization under a fixed load is rarely realistic. Multiload approaches consider a fixed (usually small) number of different loading configurations and have been developed for example in [3, 30] and references therein. In this paper, we deal with stochastic loading and risk averse optimization. Optimization under uncertainty requires an appropriate treatment of the available uncertain data information. Different approaches have been analyzed, which are appropriate for different types of risk. Robust optimization corresponds to a treatment of the worst-case [15] and is based on information about the ranges of the uncertain parameters. Applications to shape optimization can be found in [8, 22]. In stochastic optimization data uncertainty, typically quantified by probability distributions, has been largely studied in a finite-dimensional setting, both in a linear situation for mixed-integer and other nonlinear models, see for example [42]. Shape optimization with stochastic loading has been discussed previously in various contexts, for example for beam models in [38]. A number of papers addressed worst-case optimization, see for example [4, 8, 16] and the optimization scenario in aerodynamic design in [43]. A trust-region algorithm for PDE optimization under uncertainty was developed in [37]. In [25] we have proposed an efficient optimization approach for stochastic loading based on the representation of realizations of surface and volume loads as linear combinations of a few basis modes. In our previous work [25, 26, 28] we have shown how this approach can be used to effectively perform shape optimization with different treatments of the stochastic loads.

3 Elasticity of Micro Perforated Elastic Material

We consider here an elastic body composed of microstructured material and suppose that the microstructure is composed of mechanically constructible perforations. On the microscale these perforations form a regular lattice, which is not necessarily oriented parallel to the macroscopic axes. The geometry of these perforations and the orientation of the lattice vary macroscopically and are locally described by a finite set of parameters.

Before we investigate a computationally feasible two-scale formulation let us discuss the case of an elastic object with perforation on a fine scale lattice with regular lattice spacing $\delta > 0$, as illustrated in Fig. 1. We denote by $D \subset \mathbb{R}^d$ the underlying object domain, connected, with Lipschitz boundary and suppose that $\Gamma_D \subset \partial D$ is the Dirichlet boundary where the elastic object is fixated and $\Gamma_N \subset \partial D$ the Neumann boundary on which boundary forces are applied. We suppose that Dirichlet and Neumann boundaries are relatively open subsets of ∂D with Lipschitz boundary, the first one nonempty. The elastic object itself is perforated with holes of size less than δ drilled into homogeneous elastic bulk material on D and described by the perforated domain $D_\alpha^\delta = D \setminus \left(\bigcup_{x \in \delta\mathbb{Z}^d} x + \delta \mathfrak{m}_{\alpha(x)}\right)$. Here, $\mathfrak{m}_{\alpha(x)} \subset [-\gamma, \gamma]^d$ with γ fixed and $0 < \gamma < \frac{1}{2}$ describes the geometry of the perforation placed at $x \in \delta\mathbb{Z}^d$ and defined on the reference domain $[-\frac{1}{2}, \frac{1}{2}]^d$ for a parameter function $\alpha : D \to \mathbb{R}^m$ with $m \in \mathbb{N}$. We denote by $\mathcal{U}_{\text{ad}}$ a closed set of admissible parameters such that $\alpha(x) \in \mathcal{U}_{\text{ad}}$ for every $x \in D$. Let us assume that there are no perforations close to the Dirichlet and Neumann boundary, i. e. $\mathfrak{m}_{\alpha(x)} = \emptyset$ for $\text{dist}(x, \Gamma_D \cup \Gamma_N) \leq \Delta$ for some fixed $\Delta > 0$. For a displacement $u^\delta : D_\alpha^\delta \to \mathbb{R}^d$ and a boundary force density $g : \Gamma_N \to \mathbb{R}^d$ the elastic energy is given by

$$E^\delta[\alpha, u^\delta] = \frac{1}{2} \int_{D_\alpha^\delta} \mathbf{C}(x) \epsilon[u^\delta](x) : \epsilon[u^\delta](x) \, \mathrm{d}x - \int_{\Gamma_N} g(x) \cdot u^\delta(x) \, \mathrm{d}a$$

where $\mathbf{C}$ is the elasticity tensor of the homogeneous bulk material, $\epsilon[\phi] = \frac{1}{2}(\mathbf{D}\phi + \mathbf{D}\phi^T)$ denotes the strain tensor with $\mathbf{D}\phi$ being the Jacobian of the displacement ϕ and $A : B := \text{tr}(A^T B)$. If $\mathbf{C}$ is uniformly coercive and $g \in L^2(\Gamma_N, \mathbb{R}^d)$, the unique minimizer in the space $H^{1,2}_{\Gamma_D,\delta} := \{ u \in H^{1,2}(D_\alpha^\delta)^d \,|\, u = 0 \text{ on } \Gamma_D \}$ is the

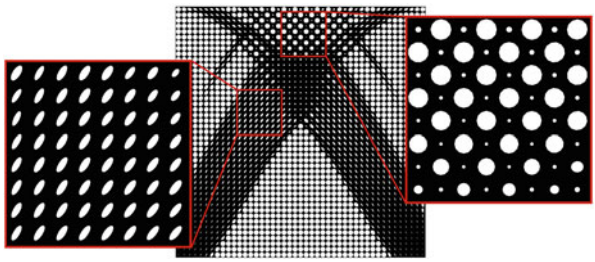

Fig. 1 Single-scale model for a carrier plate under shearing with 45×45 ellipsoidal holes. The two blow-ups show regions with locally (almost) periodic patterns

solution of the associated variational problem $\int_{D_\alpha^\delta} \mathbf{C}(x)\epsilon[u^\delta](x) : \epsilon[\phi^\delta](x)\,\mathrm{d}x = \int_{\Gamma_N} g(x)\cdot\phi^\delta(x)\,\mathrm{d}a$ for all $\phi^\delta \in H^{1,2}_{\Gamma_D,\delta}$. Figure 1 shows an elastic object with a perforation based on ellipsoidal holes where the parameters of the ellipses are optimized with respect to a compliance type cost functional.

A classical result from homogenization theory [21, 23] describes the elastic behavior of the material in the limit for $\delta \to 0$. Indeed a suitable extension of the elastic displacement u^δ onto the whole domain D converges to a displacement $u^\star \in H^{1,2}_{\Gamma_D} := \{\, u \in H^{1,2}(D)^d \mid u = 0 \text{ on } \Gamma_D \}$ which solves the variational problem

$$\int_D \mathbf{C}^\star(x)\epsilon[u^\star](x) : \epsilon[\phi](x)\,\mathrm{d}x = \int_{\Gamma_N} g(x)\cdot\phi(x)\,\mathrm{d}a \tag{3.1}$$

for all $\phi \in H^{1,2}_{\Gamma_D}$. Here, $\mathbf{C}^\star(x)$ is the effective elasticity tensor encoding the effective properties of the perforated material on the macroscale. Thereby, the underlying two-scale formulation of the limit problem is as follows. Find an effective macroscopic displacement $u^\star \in H^{1,2}_{\Gamma_D}$ and a microscopic correction $w^\star \in \mathbf{W}_\alpha$ which solve the equation

$$\int_D \int_{\mathcal{C}_\alpha(x)} \mathbf{C}(y)(\epsilon[u^\star](x) + \epsilon[w^\star](x,y)) : (\epsilon[\phi](x) + \epsilon[\psi](x,y))\,\mathrm{d}y\,\mathrm{d}x = \int_{\Gamma_N} g(x)\cdot\phi(x)\,\mathrm{d}a$$

for all $\phi \in H^{1,2}_{\Gamma_D}$ and all functions $\psi \in \mathbf{W}_\alpha$ where $\mathcal{C}_\alpha(x) := (-\frac{1}{2},\frac{1}{2})^d \setminus \mathfrak{m}_{\alpha(x)}$ and the function space of microscopic periodic displacement corrections is defined as

$$\begin{aligned}\mathbf{W}_\alpha := \{\, &\phi : (x,y) \to \phi(x,y) \in \mathbb{R}^d \mid x \in D\,,\ y \in \mathcal{C}_\alpha(x)\,,\\ &\phi(x, y+z) = \phi(x,y) \forall z \in \mathbb{Z}^d \text{ with } \|\phi\|_{\mathbf{W}_\alpha} \le \infty\}\end{aligned}$$

where $\|\phi\|_{\mathbf{W}_\alpha} := \left(\int_D \int_{\mathcal{C}_\alpha(x)} \phi(x,y)^2 + |\mathbf{D}_y\phi(x,y)|^2\,\mathrm{d}y\,\mathrm{d}x\right)^{\frac{1}{2}}$. The effective elasticity tensor $\mathbf{C}^\star = \mathbf{C}^\star[\alpha]$ can be defined variationally

$$\mathbf{C}^\star(x)\epsilon[u](x) : \epsilon[u](x) = \int_{\mathcal{C}_\alpha(x)} \mathbf{C}(y)\epsilon[R^\star[u]](x,y) : \epsilon[R^\star[u]](x,y)\,\mathrm{d}y$$

where $R^\star[u](x,y) := u(x) + w(x,y)$ for $u \in H^{1,2}_{\Gamma_D}$ is the microscopic reconstruction with w solving the correction problem $\int_{\mathcal{C}_\alpha(x)} \mathbf{C}(y)(\epsilon[u](x) + \epsilon[w](x,y)) : \epsilon[\psi](x,y)\,\mathrm{d}y = 0$ for all $\psi \in \mathbf{W}_\alpha$. Indeed, using the symmetry assumption $\mathbf{C}^\star_{ijkl} = \mathbf{C}^\star_{jikl} = \mathbf{C}^\star_{ijlk} = \mathbf{C}^\star_{klij}$, also for the effective elasticity tensor $\mathbf{C}^\star$ one observes that

$$\mathbf{C}^\star_{ijkl} = \mathbf{C}^\star\epsilon_{ij} : \epsilon_{kl} = \mathbf{C}^\star\epsilon_{ij+kl} : \epsilon_{ij+kl} - \mathbf{C}^\star\epsilon_{ij-kl} : \epsilon_{ij-kl} \tag{3.2}$$

with $\epsilon_{ij} = \frac{1}{2}(e_i \otimes e_j + e_j \otimes e_i)$ and $\epsilon_{ij\pm kl} = \frac{1}{2}(\epsilon_{ij} \pm \epsilon_{kl})$ where e_i is the ith canonical basis vector in $\mathbb{R}^d$. Thus, for every $x \in D$ one evaluates the reconstruction $R^\star$ for a basis of affine displacements and then via the above representation the coefficients of the effective elasticity tensor $\mathbf{C}^\star_{ijkl}$ for all $1 \le i, j, k, l \le d$.

In shape optimization it turns out to be advantageous to allow also spatially varying orientation of the microscopic perforation pattern, for which the microscopic perforation $\mathfrak{m}_{\alpha(x)}$ is no longer contained in $[-\gamma, \gamma]^d$. This enlarges substantially the class of possible microstructures which can be achieved without increasing much the number of parameters. To this end, we allow for a rotation $Q(\alpha(x))$ of the microscopic cell $x + \delta[-\frac{1}{2}, \frac{1}{2}]^d$ depending on the local value $\alpha(x)$ of the macroscopic parameter function and use $\mathcal{C}_\alpha(x) = Q(\alpha(x))(-\frac{1}{2}, \frac{1}{2})^d \setminus \mathfrak{m}_{\alpha(x)}$ in the definition of the two-scale approach above. Furthermore, we have to adopt the definition of $\mathbf{W}_\alpha$ using the rotated periodicity assumption $\phi(x, y + z) = \phi(x, y) \forall z \in Q(\alpha(x))\mathbb{Z}^d$. Let us emphasize that in this case the fine scale problem on a scale δ need not be properly defined any longer.

In this paper we will compare the performance of different types of microscopic perforations on two dimensional domains ($d = 2$). In what follows we will describe the associated parametrization (cf. Fig. 2):

- *Cells with single ellipsoidal holes.* An ellipsoidal shaped hole is considered, parametrized by the lengths $\alpha_1, \alpha_2 \in (0, \gamma)$ of its two semiaxes and a rotation α_3 (cf. Fig. 1).
- *Cells with* 2×2 *ellipsoidal holes.* A natural extension is achieved by allowing 2×2 holes with 12 independent parameters per cell.
- *Cell structures consisting of axes-aligned trusses.* As an alternative construction we consider truss like structures along the edges and the diagonals of the cell, where the thickness α_i ($i = 1, \ldots, 6$) can be varied. Additional constraints make sure that the holes generated between the trusses maintain a triangular shape.
- *Cell structures consisting of freely rotated orthogonal trusses.* Finally two orthogonal trusses connecting midpoints of opposing edges of the cell are allowed to rotate freely. This periodic pattern is equivalently determined by the rectangular hole centered at the corners of the cell and parametrized by the half edge lengths $\alpha_1, \alpha_2 \in (0, \gamma)$ and an unconstrained rotation α_3.

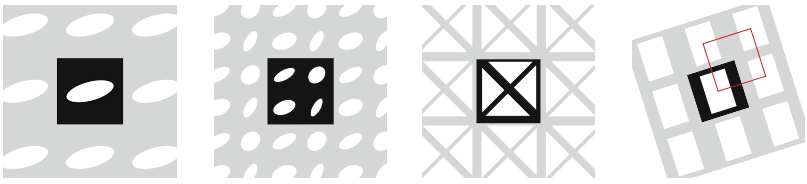

Fig. 2 Form left to right the different cells with different type of perforation are displayed: cells with single ellipsoidal holes, cells with 2×2 ellipsoidal holes, cell structures consisting of axes aligned and diagonal trusses, freely rotated cells with rectangular holes representing orthogonal trusses (see *red marking*)

All parametrizations described above lead to perforations of the fundamental cell leaving behind a certain amount of rigid constituent. The fraction $\theta(x) = \mathrm{Vol}(\mathcal{C}_\alpha(x))$ can be interpreted as the macroscopic local density of the effective material. To rule out trivial solutions to the shape optimization problem we impose a global volume constraint. The total amount of material spent $\Theta = \int_D \theta(x)\,\mathrm{d}x$ is to be kept fixed throughout the optimization procedure.

In the implementation of our two-scale simulation method we use a finite element scheme on the macroscale and a boundary element scheme on the microscale (cf. Sect. 5).

4 Two-Scale Shape Optimization Under Stochastic Loadings

For every choice of the parameter function α we can compute a corresponding macroscopic displacement $u^\star[\alpha]$. Given a cost functional $\mathbf{J}$, which may depend directly on the parameter function α and the macroscopic displacement $u^\star$, we ask for an optimal shape, described via macroscopically parametrized microscopic perforations. Precisely, we want to compute a parameter function α which minimizes $\mathcal{J}[\alpha] := \mathbf{J}[\alpha, u^\star[\alpha]]$. Before dealing with stochastic shape optimization we briefly discuss the deterministic case.

Deterministic shape optimization In this article we will focus on the compliance cost functional as a global measure of rigidity. We can write the resulting cost in the following equivalent ways (cf. (3.1)):

$$\mathbf{J}[\alpha, u] = \int_{\Gamma_N} g(x)\cdot u(x)\,\mathrm{d}a = \int_D \mathbf{C}^\star[\alpha](x)\,\varepsilon[u](x) : \varepsilon[u](x)\,\mathrm{d}x\,. \tag{4.1}$$

The derivative $\mathcal{J}'[\alpha]$, which plays in our context the role of the shape derivative, takes the form $\mathcal{J}'[\alpha] = \mathbf{J}_{,\alpha}[\alpha, u^\star[\alpha]] + \mathbf{J}_{,u}[\alpha, u^\star[\alpha]](\partial_\alpha u^\star[\alpha])$, where $\mathbf{J}_{,\alpha}[\alpha, u^\star[\alpha]] = \int_D \partial_\alpha \mathbf{C}^\star[\alpha](x)\epsilon[u^\star[\alpha]](x) : \epsilon[u^\star[\alpha]](x)\,\mathrm{d}x$. To avoid computing sensitivities $\partial_\alpha u^\star[\alpha]$ of the displacement w.r.t. the perforation parameter function α we employ the dual problem. Here, the dual solution $p^\star = p^\star[\alpha] \in H^{1,2}_{\Gamma_D}$ is defined as the weak solution of

$$\int_D \mathbf{C}^\star[\alpha](x)\epsilon[p^\star](x) : \epsilon[\phi](x)\,\mathrm{d}x = -\mathbf{J}_{,u}[\alpha, u^\star[\alpha]](\phi) \tag{4.2}$$

for all $\phi \in H^{1,2}_{\Gamma_D}$. In our case of a compliance type cost functional $p^\star[\alpha] = -2u^\star[\alpha]$. With the dual solution at hand one can rewrite the derivative of the cost

$$\begin{aligned}\mathcal{J}'[\alpha] &= \mathbf{J}_{,\alpha}[\alpha, u^\star[\alpha]] + \int_D \left(\partial_\alpha \mathbf{C}^\star[\alpha]\right)(x)\epsilon[u^\star[\alpha]](x) : \epsilon[p^\star[\alpha]](x)\,\mathrm{d}x \\ &= -\int_D \left(\partial_\alpha \mathbf{C}^\star[\alpha]\right)(x)\epsilon[u^\star[\alpha]](x) : \epsilon[u^\star[\alpha]](x)\,\mathrm{d}x\,.\end{aligned} \tag{4.3}$$

Finally, we are left to compute $\partial_\alpha \mathbf{C}^\star[\alpha](x)$ for $x \in D$. To this end, taking into account (3.2) we consider $\mathbf{C}^\star[\alpha](x)\varepsilon_{ij\pm kl} : \varepsilon_{ij\pm kl}$ for fixed i, j, k, l and for fixed $x \in D$ and define the local cost functional $j_C[\alpha] = \mathbf{j}_C[\alpha, w^\star_{ij\pm kl}[\alpha]]$ with $\mathbf{j}_C[\alpha, w] = \int_{C_\alpha(x)} \mathbf{C}(y)\left(\varepsilon_{ij\pm kl} + \varepsilon[w](x,y)\right) : \left(\varepsilon_{ij\pm kl} + \varepsilon[w](x,y)\right) \mathrm{d}y$ and $w^\star_{ij\pm kl}[\alpha](x,\cdot)$ is given as the solution of the local correction problem $0 = \int_{C_\alpha(x)} \mathbf{C}(y)\left(\varepsilon_{ij\pm kl} + \varepsilon[w](x,y)\right) : \varepsilon[\psi](x,y)\,\mathrm{d}y$ for all $\psi \in \mathbf{W}_\alpha$ and with x being fixed. This implies

$$\mathbf{j}_C[\alpha, w^\star_{ij\pm kl}[\alpha]] = \int_{C_\alpha(x)} \mathbf{C}(y)\left(\varepsilon_{ij\pm kl} + \varepsilon[w^\star_{ij\pm kl}[\alpha]](x,y)\right) : \left(\varepsilon_{ij\pm kl} + \varepsilon[w^\star_{ij\pm kl}[\alpha]](x,y)\right) \mathrm{d}y\,.$$

From the correction problem we immediately deduce that $\partial_w \mathbf{j}_C[\alpha, w^\star_{ij\pm kl}[\alpha]] = 0$. Hence, one obtains $\partial_\alpha j_C[\alpha] = \partial_\alpha \mathbf{j}_C[\alpha, w^\star_{ij\pm kl}[\alpha]]$. Taking into account a family of perforations defined via the mapping $s \mapsto \mathfrak{m}_{\alpha(x)+s\beta}$ for $s \in \mathbb{R}$ with $|s|$ small, we then obtain for the variation of the local cost $j_C[\alpha]$ in direction $\beta \in \mathbb{R}^m$

$$\begin{aligned}\partial_\alpha j_C[\alpha](\beta) &= \frac{\mathrm{d}}{\mathrm{d}s} j_C[\alpha + s\beta]\Big|_{s=0} = \frac{\mathrm{d}}{\mathrm{d}s}\mathbf{j}_C[\alpha + s\beta, w^\star_{ij\pm kl}[\alpha]]\Big|_{s=0} \\ &= \int_{\partial\mathfrak{m}_{\alpha(x)}} (v_{\alpha,\beta}(y)\cdot n_{\partial\mathfrak{m}_{\alpha(x)}}(y))\mathbf{C}(y)\left(\varepsilon_{ij\pm kl} + \varepsilon[w^\star_{ij\pm kl}[\alpha]](x,y)\right) : \\ &\qquad \left(\varepsilon_{ij\pm kl} + \varepsilon[w^\star_{ij\pm kl}[\alpha]](x,y)\right) \mathrm{d}y\end{aligned}$$

where $n_{\partial\mathfrak{m}_{\alpha(x)}}(y)$ denotes the inner normal of the perforation $\mathfrak{m}_{\alpha(x)}$ at $y \in \partial\mathfrak{m}_{\alpha(x)}$ and $v_{\alpha,\beta}(y)$ is the velocity vector associated with the variation of $\mathfrak{m}_{\alpha(x)}$ in the direction β at position $y \in \partial\mathfrak{m}_{\alpha(x)}$. Finally, we obtain for the variation of the effective elasticity tensor in a direction $\beta \in \mathbb{R}^m$

$$\begin{aligned}&\partial_\alpha \mathbf{C}^\star_{ijkl}[\alpha](\beta) = \\ &\int_{\partial\mathfrak{m}_{\alpha(x)}} \mathbf{C}(y)\Big(\left(\varepsilon_{ij+kl} + \varepsilon[w^\star_{ij+kl}](x,y)\right) : \left(\varepsilon_{ij+kl} + \varepsilon[w^\star_{ij+kl}[\alpha]](x,y)\right) - \\ &\qquad \left(\varepsilon_{ij-kl} + \varepsilon[w^\star_{ij-kl}](x,y)\right) : \left(\varepsilon_{ij-kl} + \varepsilon[w^\star_{ij-kl}[\alpha]](x,y)\right)\Big) \\ &\qquad \cdot\, (v_{\alpha,\beta}(y)\cdot n_{\partial\mathfrak{m}_{\alpha(x)}}(y))\,\mathrm{d}y\,.\end{aligned}$$

Two-stage stochastic shape optimization In a more realistic situation the actual loading of an elastic work piece is usually not fixed but varies stochastically. Therefore we now extend the above framework and consider random surface loads $g(\omega) \in L^2(\Gamma_N;\mathbb{R}^d)$ with ω being a realization on an abstract probability space $(\Omega, \mathcal{A}, \wp)$. Here, finite-dimensional linear stochastic programs serve as blueprints for our stochastic shape optimization models. In this context a two-stage scheme of alternating decision and observation applies. The first-stage decision of a concrete shape, in our context the parameter vector α, must not anticipate future information

on the random data, here the random boundary force $g(\omega)$. The second-stage decision in our context corresponds to the solution of the elastic problem and the evaluation of the cost value for a concrete realization ω and for fixed α and $g(\omega)$. The overall aim of two-stage stochastic programming is to find an α which is in a stochastic sense "optimal" under these circumstances. Different modes of ranking random variables then lead to different types of stochastic programs. In a risk neutral setting the ranking is done by taking the expectation $\mathbb{E}_\omega$. With risk aversion, see [17, 41] for a recent textbook and a monograph as well as the journal publications [27, 39, 44], expectation is replaced by statistical parameters reflecting some perception of risk (risk measures) or stochastic dominance relations are employed. In what follows we will focus on risk measures. For a fixed realization ω and fixed parameter function α primal and dual solutions $u[\alpha](\omega)$, $p[\alpha](\omega)$ can be computed as described above in the deterministic setting. As the solutions now depend on ω so do the associated variational problems (3.1) and (4.2) as well as the cost functional (4.1) and its gradient (4.3). Altogether we obtain the random shape optimization model $\min\{\mathbf{J}[\alpha, u, \omega] : \alpha \in \mathcal{U}_{\mathrm{ad}}\}$, which amounts to finding a "minimal" member in the family of random variables $\mathbf{J}[\alpha, u, \omega]$. Taking the expectation yields the risk neutral problem $\min\{\mathbf{Q}_{\mathrm{EV}}[\alpha] := \mathbb{E}_\omega(\mathbf{J}[\alpha, u, \omega]) : \alpha \in \mathcal{U}_{\mathrm{ad}}\}$. Risk averse problems are the expected excess $\min\left\{\mathbf{Q}_{\mathrm{EE}_\eta}[\alpha] := \mathbb{E}_\omega(\max\{\mathbf{J}[\alpha, u, \omega] - \eta, 0\}) : \alpha \in \mathcal{U}_{\mathrm{ad}}\right\}$ or the excess probability $\min\left\{\mathbf{Q}_{\mathrm{EP}_\eta}[\alpha] := \mathbb{P}_\omega(\mathbf{J}[\alpha, u, \omega] > \eta) : \alpha \in \mathcal{U}_{\mathrm{ad}}\right\}$ over a preselected target $\eta \in \mathbb{R}$. For the numerical realization we will use smooth approximations of the max-function and the Heaviside function leading to $\mathbf{Q}^\varepsilon_{\mathrm{EE}_\eta}[\alpha] := \mathbb{E}_\omega\left(q^\varepsilon(\mathbf{J}[\alpha, u, \omega])\right)$, where $q^\varepsilon(t) := \frac{1}{2}(\sqrt{(t-\eta)^2 + \varepsilon} + (t - \eta))$ and $\mathbf{Q}^\varepsilon_{\mathrm{EP}_\eta}[\alpha] := \mathbb{E}_\omega\left(H^\varepsilon(\mathbf{J}[\alpha, u, \omega])\right)$ with $H^\varepsilon(t) := (1 + e^{-\frac{2(t-\eta)}{\varepsilon}})^{-1}$ for $\varepsilon > 0$. For actual computations $(\Omega, \mathcal{A}, \wp)$ is assumed to be finite, in the sense that there are finitely many realizations ω_i and probabilities π_i, $i = 1, \ldots, N_s$. We can then rewrite $\mathbf{Q}_{\mathrm{EV}}[\alpha] = \sum_{i=1}^{N_s} \pi_i \mathbf{J}[\alpha, u, \omega_i]$, and $\mathbf{Q}^\varepsilon_{\mathrm{EE}_\eta}[\alpha]$ and $\mathbf{Q}^\varepsilon_{\mathrm{EP}_\eta}[\alpha]$ accordingly. The shape derivative as derived above can directly be applied to the stochastic functionals. The chain rule yields

$$
\begin{aligned}
\mathbf{Q}'_{\mathrm{EV}}[\alpha](\beta) &= \sum_{i=1}^{N_s} \pi_i \, \mathbf{J}'[\alpha, u, \omega_i](\beta)\,, \\
(\mathbf{Q}^\varepsilon_{\mathrm{EE}_\eta})'[\alpha](\beta) &= \sum_{i=1}^{N_s} \tfrac{\pi_i}{2} \mathbf{J}'[\alpha, u, \omega_i](\beta) \left(\frac{\mathbf{J}[\alpha,u,\omega_i]-\eta}{\sqrt{(\mathbf{J}[\alpha,u,\omega_i]-\eta)^2+\varepsilon}} + 1 \right), \\
(\mathbf{Q}^\varepsilon_{\mathrm{EP}_\eta})'[\alpha](\beta) &= \sum_{i=1}^{N_s} \tfrac{2}{\varepsilon} \pi_i \mathbf{J}'[\alpha, u, \omega_i](\beta) \, \frac{e^{-\frac{2}{\varepsilon}(\mathbf{J}[\alpha,u,\omega_i]-\eta)}}{\left(1+e^{-\frac{2}{\varepsilon}(\mathbf{J}[\alpha,u,\omega_i]-\eta)}\right)^2}
\end{aligned}
$$

for a direction $\beta : D \to \mathbb{R}^m$ in which α is varied. So far it seems that for every ω_i one has to compute a primal and a dual solution. The solution, however, depends linearly on the right hand side; therefore a significant amount of computational time can be spared when a large number N_s of scenarios is generated by a small set

of basis surface loads $g_1, \dots, g_K$, as was discussed in [25]. The actual loads $g(\omega)$ are given as linear combinations $g(\omega) = \sum_{j=1}^{K} \lambda_j(\omega) g_j$, with random coefficients $\lambda_j(\omega) \in \mathbb{R}$, $j = 1, \dots, K$. We thus only need to solve the elasticity problem for the different basis forces. To be more precise let $u^{j,\star}[\alpha]$ be the solution of (3.1) for $g = g_j$, $j = 1, \dots, K$. Then we find $u^\star[\alpha](\omega) := \sum_{j=1}^{K} \lambda_j(\omega)\, u^{j,\star}[\alpha]$ to be the unique solution of (3.1) with $g = g(\omega)$. The same procedure can be taken for the dual solution if the cost functional is at most quadratic guaranteeing the linearity in the right hand side. As discussed, in our case of a compliance objective the dual problem is already trivial.

5 Implementation

The two-scale simulation is based on a finite element discretization on the macroscale and a boundary element method on the microscale. We use a regular mesh with N quadratic cells on the macroscale and piecewise biquadratic finite elements as checkerboard instabilities were reported in [18] for the related case of nested laminates when using linear ansatz functions. We use a Gaussian quadrature of consistency order 5 with 3×3 quadrature points per square cell. Within each cell the underlying microstructure is specified by a set of parameters in $\mathbb{R}^m$ as the discrete counterpart of the local parameter function α. For the cell problem a collocation type boundary element method is used to compute numerical approximations to the microscopic correction profiles. For details we refer to the corresponding discussion for the single-scale model in [6]. The design constraints described in Sect. 3 are implemented as inequality constraints in the optimization. The global volume constraint leads to an additional equality constraint. Unless otherwise noted we use a material with moderate anisotropy for the construction of microscopic geometries. It is characterized by the elasticity tensor

$$\mathbf{C}_{\text{aniso}} = \begin{pmatrix} 3 & 1 & & \\ 1 & 3 & & \\ & & 1.1 & \end{pmatrix}$$

using Voigt's notation. For all numerical experiments we prescribe a volume fraction of 67 % as global constraint. Loads usually have magnitude 1.

Our algorithm for the two-scale shape optimization approach is written in `C++` based on the `quocmesh` library for finite element and boundary element computations and the open source software `Ipopt` [47,48] performing constrained finite-dimensional optimization.

6 Numerical Results

In this section we present numerical results for shape optimization problems both with deterministic and stochastic loadings, comparing the different microstructure models. The key scenario we consider is a carrier plate, in which the computational domain is the unit square, with homogeneous Dirichlet boundary data on the bottom and Neumann boundary conditions corresponding to a shearing on the top. To illustrate the generality of the method we also study two classical problems from the literature.

6.1 Deterministic Optimization

We start with the simplest microstructure, in which every unit cell has one ellipsoidal hole (first sketch in Fig. 2). The results for the three model problems discussed above are presented in Fig. 3 based on computations on a macroscopic grid with 64×64 square cells.

Comparing the results for the carrier plate scenario to the single-scale case illustrated in Fig. 1 a remarkable similarity is apparent. The oscillating pattern observed in the single-scale case (Fig. 1, left blow-up) for the upper middle region however seems to be gone. The apparent reason for these oscillations was to approximate criss-crossing beams. Such a construction is ruled out by the kinematics in the two-scale setting, since each unit cell only contains one hole, which then gets repeated over and over again at the microscale.

This suggests to allow for more than one hole within the fundamental cell, each with its own set of parameters. We investigated this structure using 2×2 holes on each cell, which is the microstructure sketched in the second panel of Fig. 2. In the result, see Fig. 4c, the oscillating pattern is now captured as expected while other regions keep their microstructure by just reproducing the shape of the former single hole four times.

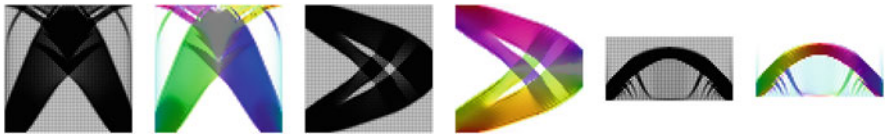

Fig. 3 Local minima for two-scale optimization of a carrier plate under shearing, a cantilever on a square domain and a bridge scenario, all on a macroscopic regular rectangular mesh with 64×64 cells. The local configuration is drawn within each macroscopic element as a representative for the underlying microstructure. Furthermore, the same results are presented using a HSV color code: color corresponds to the rotation of the major semiaxis, saturation to the degree of anisotropy and value to the volume of the hole

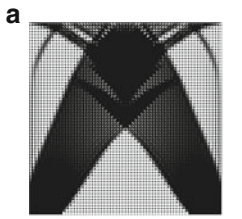

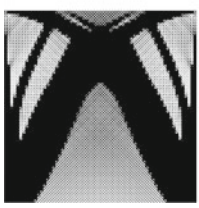

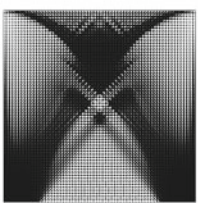

f

Structure	**J**
(a)	2.0358
(b)	2.0255
(c)	2.0276
(d)	1.8959
(e)	1.8122

Fig. 4 Local minima for two-scale optimization of a carrier plate under shearing for different configurations: (**a**) 64×64 macroscopic cells with 1 ellipsoidal hole each (same as in Fig. 3), (**b**) 128×128 macroscopic cells with 1 ellipsoidal hole each, (**c**) 64×64 macroscopic cells with 2×2 ellipsoidal holes each, (**d**) 64×64 macroscopic cells with 6 trusses at fixed positions each, and (**e**) 64×64 macroscopic cells with 2 rotated orthogonal trusses each. Final objective values are listed in (**f**)

Since we already conjectured that a framework with diagonal trusses would perform best in the upper middle region, we now explicitly consider such a microstructure. First we place six trusses at fixed positions within the fundamental cell (third panel in Fig. 2). In the resulting shape, see Fig. 4d, the expected criss-crossing pattern is found. However we now see solid trusses in the macroscopic picture. This is because the optimal shape has trusses which are not inclined by 45° and therefore cannot be reproduced by the microstructure; the optimization hence generates "macroscopic trusses" with the appropriate slope. This suggests to allow for a rotation of the whole periodic lattice (fourth panel in Fig. 2). The results are shown in Fig. 4e. The last panel of Fig. 4 gives an overview of the final objective values for the optimized designs. One can clearly see that the improvement of the shape by allowing a more complex microstructure using 2×2 holes per cell becomes manifest also in a quantitative way. The introduction of structures made from fixed trusses leads to a further significant drop in the objective functional. Finally allowing the structures to rotate freely again contributes to a substantial improvement.

So far we have successively constructed microscopic geometries that lead to a stepwise reduction in the objective value for the optimized design. It seems natural to compare the results to a microstructure that is known to be optimal a priori. For our comparison we decided to adopt the nested laminates construction as it is valid on the full range of feasible strains and explicit formulae as well as an algorithmic treatment are available in [1]. The microstructure is built up in an iterative procedure. One starts by successively layering a given rigid and a very weak material, determined by elasticity tensors B and A respectively, with proportions

m_1 and $(1 - m_1)$ in a direction e_1. The obtained material is then layered again with the rigid material B, now with proportion m_2 and in direction e_2. In our shape optimization context one considers the degenerate case in which the weak material A is replaced by voids. By a limiting process the effective elasticity tensor $\mathbf{C}_L^\star$ of the nested laminate can be given in closed form with the ratios m_1, m_2, the directions e_1, e_2, and the overall material density θ as degrees of freedom [1]. Moreover, these parameters depend explicitly on the local effective stress $\sigma^\star = \mathbf{C}_L^\star u^\star$. Indeed, the ratios m_1 and $m_2 = 1 - m_1$ are given by the ratio of the eigenvalues of $\sigma^\star$ and the directions e_1 and e_2 are aligned with the orthogonal system of eigenvectors. Finally using a Lagrange multiplier approach also the optimal local density θ depends, apart from elastic constants, only on the eigenvalues.

The variational structure of the problem and the values of the objective function listed in Fig. 4f give a clear ordering in the quality of the different microstructure patterns and show in particular that the rotated orthogonal trusses are superior to the other models considered, at least in the present scenario. To assess how much room for improvement is left we compare with the lower bound given by the Hashin-Shtrikman formula, focusing for simplicity on the case of an isotropic material. In the present setting this lower bound is known to be optimal and can indeed be attained by lamination [1,7]. To this end we reimplemented the alternating algorithm for the nested lamination construction proposed in [1]. The local density of the optimal structure obtained in the carrier plate scenario is compared in Fig. 5b with the result of our two-scale method for perforated isotropic material. The latter has been computed with the isotropic elasticity tensor

$$\mathbf{C}_{\text{iso}} = \begin{pmatrix} 3 & 1 & \\ 1 & 3 & \\ & & 1 \end{pmatrix}$$

in which the lower right entry was replaced by 1.0001, since we use in our boundary element scheme a fundamental solution for anisotropic elasticity. The perforation pattern in Fig. 5a is qualitatively very similar to the one obtained with anisotropic elasticity in Fig. 4e, the quantitative values of the objective function, however, differ

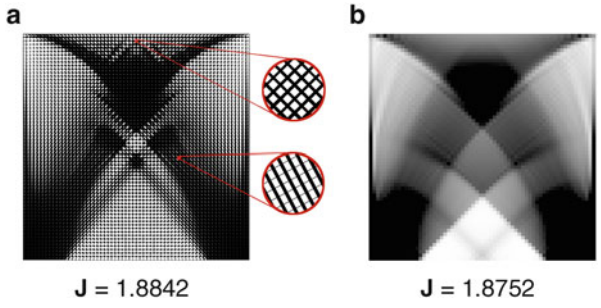

Fig. 5 A comparison of the computed optimal pattern for a carrier plate under shearing is displayed. The computations are performed on a 64 × 64 grid: (**a**) shows the microstructure composed of rotated orthogonal trusses, and (**b**) renders the density in the case of sequential laminates. The values of the objective function are listed below

significantly. The comparison of Fig. 5a, b demonstrates that the performance of the two-scale approach with rotated orthogonal trusses is indeed very close to the one of the optimal microstructure, which can be realized for example by the construction with second-order laminates. Analytically, it is known that in the low-volume-fraction limit the construction with single-scale laminates is optimal [19]. Single-scale laminates are, in the definition of [19], structures in which thin trusses with different orientations coexist without interacting; for low volume fraction and second-order laminates they correspond to our rotated trusses. The present results show that rotated trusses give almost the same objective function as laminates even for a total volume fraction of 67 %, at least in this geometry.

6.2 *Risk Averse Stochastic Optimization*

In this section we show that our developed two-scale algorithm can directly be applied to the more general situation of stochastic shape optimization. We consider a variant of the carrier plate scenario with sets of different loads on the upper left and upper right edge with different probabilities, as illustrated in Fig. 6 and described in the figure caption, similar to the one that was studied for single-scale stochastic shape optimization in [26]. For the optimization we consider both the risk neutral and the risk averse cost functionals introduced in Sect. 4. In this stochastic optimization we focus on the simplest choice of microstructure, the ellipsoidal holes, and on the one that performed best in the deterministic setting, the rotated trusses.

Figure 6 shows the result of the deterministic optimization using the expected value of the loads. The larger probability of the forces on the right results in a larger expected value of the force, and hence on a strong concentration of the available

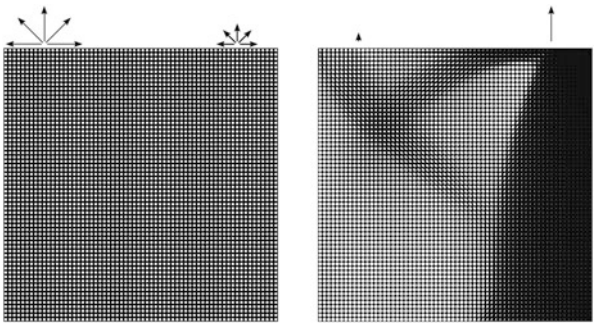

Fig. 6 *Left panel*: configuration used in the stochastic optimization. The lower boundary has homogeneous Dirichlet boundary conditions. The possible forces on the left have a probability of 1 %, those on the right 19 %. *Right panel*: result of the deterministic optimization using the expected value of loads and the ellipsoidal holes microstructure

mass on the right-hand side of the computational domain. The (on average!) minor forces on the left-hand side are dealt with by two small trusses which connect the main pillar to the other side of the domain.

In Fig. 7 we compare, using the microstructure of rotated orthogonal trusses, three different approaches to the forcing. In Fig. 7a we show the optimization of the expected value of the costs, in which both left and right forcing play a significant role. In particular, the presence of a scenario with forcing only on the left-hand side generates a substantial mass on the left-hand side of the computational domain. Figure 7b illustrates the result of optimizing w.r.t. the expected value of the loads. The two types of microstructures lead to similar shapes. In Fig. 7c we show, for a comparison, the result of the optimization in the symmetric case, with the same forces acting on both parts of the top boundary.

We now turn to the optimization of the expected excess. Figure 8 shows the results for ellipsoidal holes and rotated trusses, respectively. As in the previous case, the two types of microstructure generate similar patterns. Introducing a threshold makes the largest deviations more important, and therefore the forces on the left, which are large but have a small probability, become more important in the optimization. Indeed, for small η (and for the EV optimization) the forces on the right-hand side dominate, and correspondingly the largest structures are the vertical one on the right (which takes care of the vertical component of the forces on the right) and the diagonal from the lower left to the upper right corner (which takes care of the horizontal component of the forces on the right). With increasing η the situation becomes first symmetric, and then tilted in the other direction, with the left side and the lower right to upper left diagonal dominant at $\eta = 0.0005$.

In the case of the optimization of the excess probability, only the probability, and not the amplitude, of the large deviations plays a role. Results are shown with ellipsoidal holes for the microstructure in Fig. 9. Indeed, for small η the best result the optimization can achieve is to keep the cost functional in the scenarios corresponding to the small forces on the right-hand side below the threshold; in order to do this the small probability forces on the left-hand side are given up. The cost of these forces would, in the ideal case, be infinite (it is not due to the many

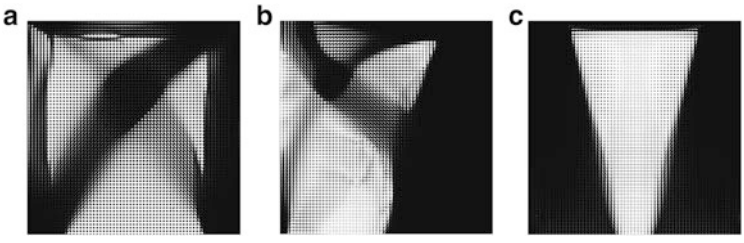

Fig. 7 Results of the two-scale shape optimization procedure using rotated trusses for the microstructure: stochastic optimization of the expected value of costs (**a**), deterministic optimization using the expected value of the loads (**b**), deterministic optimization computed for equal loads on the left and right parts (**c**)

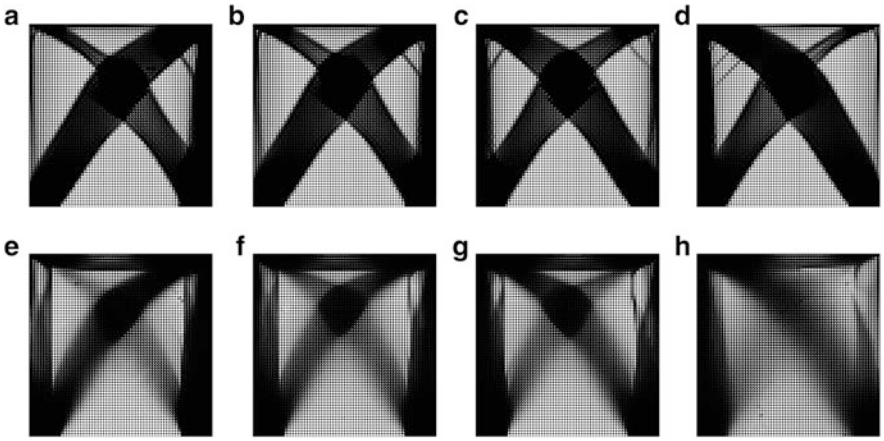

Fig. 8 Results of the two-scale stochastic optimization of the expected excess for different values of the threshold η, using ellipsoidal holes (*top*) and rotated trusses (*bottom*) for the microstructure. (**a**) EV. (**b**) $\eta = 0.0001$. (**c**) $\eta = 0.0003$. (**d**) $\eta = 0.0005$. (**e**) $\eta = 0.0001$. (**f**) $\eta = 0.0002$. (**g**) $\eta = 0.0003$. (**h**) $\eta = 0.0005$

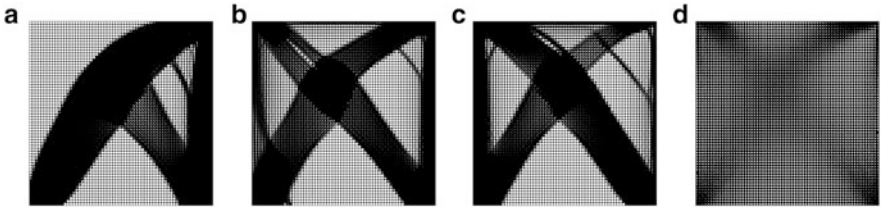

Fig. 9 Results of the two-scale stochastic optimization of the excess probability for different values of the threshold η, using ellipsoidal holes for the microstructure. (**a**) $\eta = 0.0003$. (**b**) $\eta = 0.0004$. (**c**) $\eta = 0.0005$. (**d**) $\eta = 0.0006$

numerical regularizations, including for example the fact that the volume fraction cannot be zero in any cell). This divergence does not, however, result in a divergence of the total cost functional because only the probability of these large deviations enters the optimization, not their amplitude. With increasing η, it is less important to keep the response to the small forces very small: as above, the thresholding makes the exact value of the cost functional in that case irrelevant, as long as it is below threshold. The optimization can devote material to improving the response to the forces on the left. Since they are large (but unlikely) more material is needed to bring them below threshold than for the smaller forces on the right, hence the pattern also in this case changes to a left-dominated one. When the threshold η becomes larger and larger, it is easy to keep the response to all 10 forces below it, and the problem degenerates: in a sense, there is "too much material" to achieve the aim, and the

details of the shapes are not any more meaningful. We stress that the discontinuity of the excess probability has been regularized in the numerics, hence the transitions discussed are to be interpreted as gradual transitions, not as abrupt discontinuities from "above threshold" to "below threshold".

In closing we remark that, although the details of the shapes differ, the qualitative trends we discussed are very similar to the ones we had observed in the single-scale computations in [26].

Conclusions

In this paper we derived a two-scale framework for shape optimization in which the parameters of microscopic perforations on a locally periodic lattice are optimized. We compare the performance of different types of perforation geometries and demonstrate that the best performing geometry of locally rotated orthogonal trusses gets very close to the known optimal approach based on nested lamination construction on the microscale. Furthermore, we studied stochastic shape optimization in the class of two-scale materials with approximate models for expected excess and the excess probability as risk averse cost functionals.

Acknowledgements The authors would like to thank Martin Lenz for help with the boundary element method applied to microscopic cell problems. This work was supported by the Deutsche Forschungsgemeinschaft through the Schwerpunktprogramm 1253 *Optimization with Partial Differential Equations*.

References

1. G. Allaire, *Shape Optimization by the Homogenization Method*. Applied Mathematical Sciences, vol. 146 (Springer, New York, 2002)
2. G. Allaire, E. Bonnetier, G. Francfort, F. Jouve, Shape optimization by the homogenization method. Numer. Math. **76**, 27–68 (1997)
3. G. Allaire, F. Jouve, A level-set method for vibration and multiple loads structural optimization. Comput. Methods Appl. Mech. Eng. **194**(30–33), 3269–3290 (2005)
4. G. Allaire, F. Jouve, F. de Gournay, Shape and topology optimization of the robust compliance via the level set method. ESAIM Control Optim. Calc. Var. **14**, 43–70 (2008)
5. R. Astley, J. Harrington, K. Stol, Mechanical modelling of wood microstructure, an engineering approach. Ipenz Trans. **24**(1/EMCh), 21–29 (1997)
6. P. Atwal, S. Conti, B. Geihe, M. Pach, M. Rumpf, R. Schultz, On shape optimization with stochastic loadings, in *Constrained Optimization and Optimal Control for Partial Differential Equations*, ed. by G. Leugering, S. Engell, A. Griewank, M. Hinze, R. Rannacher, V. Schulz, M. Ulbrich, S. Ulbrich. International Series of Numerical Mathematics, vol. 160, ch. 2 (Springer, Basel, 2012), pp. 215–243
7. M. Avellaneda, Optimal bounds and microgeometries for elastic two-phase composites. SIAM J. Appl. Math. **47**(6), 1216–1228 (1987)

8. N.V. Banichuk, P. Neittaanmäki, On structural optimization with incomplete information. Mech. Based Des. Struct. Mach. **35**, 75–95 (2007)
9. C. Barbarosie, Shape optimization of periodic structures. Comput. Mech. **30**(3), 235–246 (2003)
10. C. Barbarosie, A.-M. Toader, Shape and topology optimization for periodic problems. I. The shape and the topological derivative. Struct. Multidiscip. Optim. **40**(1–6), 381–391 (2010)
11. C. Barbarosie, A.-M. Toader, Shape and topology optimization for periodic problems. II. Optimization algorithm and numerical examples. Struct. Multidiscip. Optim. **40**(1–6), 393–408 (2010)
12. C. Barbarosie, A.-M. Toader, Optimization of bodies with locally periodic microstructure. Mech. Adv. Mater. Struct. **19**(4), 290–301 (2012)
13. M. P. Bendsøe, *Optimization of Structural Topology, Shape, and Material* (Springer, Berlin, 1995)
14. M. P. Bendsøe, A. Díaz, N. Kikuchi, Topology and generalized layout optimization of elastic structures, in *Topology Design of Structures* (Sesimbra, 1992). NATO Advanced Science Institutes Series E: Applied Sciences, vol. 227 (Kluwer Academic, Dordrecht, 1993), pp. 159–205
15. A. Ben-Tal, L. El-Ghaoui, A. Nemirovski, *Robust Optimization* (Princeton University Press, Princeton/Oxford, 2009)
16. A. Ben-Tal, M. Kočvara, A. Nemirovski, J. Zowe, Free material design via semidefinite programming: the multiload case with contact conditions. SIAM J. Optim. **9**, 813–832 (1999)
17. J.R. Birge, F. Louveaux, *Introduction to Stochastic Programming*. Springer Series in Operations Research (Springer, New York, 1997)
18. E. Bonnetier, F. Jouve, Checkerboard instabilities in topological shape optimization algorithms, in *Proceedings of the Conference on Inverse Problems, Control and Shape Optimization (PICOF'98)*, Carthage, 1998
19. B. Bourdin, R.V. Kohn, Optimization of structural topology in the high-porosity regime. J. Mech. Phys. Solids **56**(3), 1043–1064 (2008)
20. A. Braides, A. Defranceschi, *Homogeneization of Multiple Integrals* (Claredon Press, Oxford, 1998)
21. G. Buttazzo, G. Dal Maso, Shape optimization for Dirichlet problems: relaxed formulation and optimality conditions. Appl. Math. Optim. **23**, 17–49 (1991)
22. A. Cherkaev, E. Cherkaev, Principal compliance and robust optimal design. J. Elast. **72**, 71–98 (2003)
23. D. Cioranescu, P. Donato, *An Introduction to Homogenization* (Oxford University Press, Oxford, 1999)
24. D. Cioranescu, J.S.J. Paulin, *Homogenization of Reticulated Structures* (Springer, New York, 1999)
25. S. Conti, H. Held, M. Pach, M. Rumpf, R. Schultz, Shape optimization under uncertainty – a stochastic programming perspective. SIAM J. Optim. **19**, 1610–1632 (2009)
26. S. Conti, H. Held, M. Pach, M. Rumpf, R. Schultz, Risk averse shape optimization. SIAM J. Control Optim. **49**, 927–947 (2011)
27. D. Dentcheva, A. Ruszczyński, Optimization with stochastic dominance constraints. SIAM J. Optim. **14**, 548–566 (2003)
28. B. Geihe, M. Lenz, M. Rumpf, R. Schultz, Risk averse elastic shape optimization with parametrized fine scale geometry. Math. Program. **141**(1–2), 383–403 (2013)
29. Y. Grabovsky, R.V. Kohn, Microstructures minimizing the energy of a two phase elastic composite in two space dimensions. I. The confocal ellipse construction. J. Mech. Phys. Solids **43**(6), 933–947 (1995)
30. J.M. Guedes, H.C. Rodrigues, M.P. Bendsøe, A material optimization model to approximate energy bounds for cellular materials under multiload conditions. Struct. Multidiscip. Optim. **25**, 446–452 (2003)
31. Z. Hashin, The elastic moduli of heterogeneous materials. Trans. ASME Ser. E. J. Appl. Mech. **29**, 143–150 (1962)

32. Z. Hashin, S. Shtrikman, A variational approach to the theory of the elastic behaviour of multiphase materials. J. Mech. Phys. Solids **11**, 127–140 (1963)
33. J. Haslinger, M. Kočvara, G. Leugering, M. Stingl, Multidisciplinary free material optimization. SIAM J. Appl. Math. **70**(7), 2709–2728 (2010)
34. P. Henning, M. Ohlberger, The heterogeneous multiscale finite element method for elliptic homogenization problems in perforated domains. Numer. Math. **113**(4), 601–629 (2009)
35. S.J. Hollister, N. Kikuchi, Homogenization theory and digital imaging: a basis for studying the mechanics and design principles of bone tissue. Biotechnol. Bioeng. **43**, 586–596 (1994)
36. V. Jikov, V. Zhikov, S. Kozlov, O. Oleinik, *Homogenization of Differential Operators and Integral Functionals* (Springer, Berlin/New York, 1994)
37. D.P. Kouri, M. Heinkenschloss, D. Ridzal, B.G. van Bloemen Waanders, A trust-region algorithm with adaptive stochastic collocation for PDE optimization under uncertainty. SIAM J. Sci. Comput. **35**(4), A1847–A1879 (2013)
38. R. Melchers, Optimality-criteria-based probabilistic structural design. Struct. Multidiscip. Optim. **23**(1), 34–39 (2001)
39. N. Miller, A. Ruszczyński, Two-stage stochastic linear programming: Modeling and decomposition. Oper. Res. **59**, 125–132 (2011)
40. F. Murat, L. Tartar, Calcul des variations et homogénéisation. In *Homogenization Methods: Theory and Applications in Physics* (Bréau-sans-Nappe, 1983). Collect. Dir. Études Rech. Élec. France, vol. 57 (Eyrolles, Paris, 1985), pp. 319–369
41. G.C. Pflug, W. Römisch, *Modeling, Measuring and Managing Risk* (World Scientific, Singapore, 2007)
42. A. Ruszczyński, A. Shapiro (Eds.), *Handbooks in Operations Research and Management Sciences, 10: Stochastic Programming* (Elsevier, Amsterdam, 2003)
43. V. Schulz, C. Schillings, On the nature and treatment of uncertainties in aerodynamic design. AIAA J. **47**, 646–654 (2009)
44. A. Shapiro, Minimax and risk averse multistage stochastic programming. Eur. J. Oper. Res. **219**, 719–726 (2012)
45. O. Sigmund, On the optimality of bone microstructure, in *IUTAM Symposium on Synthesis in Bio Solid Mechanics*, Copenhagen (Springer, 2002), pp. 221–234
46. L. Tartar, Estimations fines des coefficients homogénéisés, in *Ennio De Giorgi Colloquium* (Paris, 1983). Research notes in mathematics, vol. 125 (Pitman, Boston, 1985), pp. 168–187
47. A. Wächter, *An Interior Point Algorithm for Large-Scale Nonlinear Optimization with Applications in Process Engineering*. Phd thesis, Carnegie Mellon University, 2002
48. A. Wächter, L. Biegler, On the implementation of a primal-dual interior point filter line search algorithm for large-scale nonlinear programming. Math. Program. **106**(1), 25–57 (2006)
49. W. E, B. Engquist, Z. Huang, Heterogeneous multiscale method: a general methodology for multiscale modeling. Phys. Rev. B **67**(9), 092101–1–092101–4 (2003)
50. W. E, P. Ming, P. Zhang, Analysis of the heterogeneous multiscale method for elliptic homogenization problems. J. Am. Math. Soc. **18**(1), 121–156 (2005)